# Modal Analysis-Informed Topology Optimization for Dynamic Performance Enhancement of Horizontal Canned Motor Pumps

Xiang Sun [1], Duo Yang [1,*], Mingyan Shi [1], Gaoce Tan [1], Taomin Song [2], and Panhao Yang [3]

[1] School of Mechanical Engineering, Dalian University, Liaoning, 116622, China
[2]Army Military Representative Office, Shenyang, 110000, China
[3]Army Military Representative Office, Dalain, 116000, China
Email: 1060772585@qq.com (X.S.); yangduo@dlut.edu.cn (D.Y.); 1911214130@qq.com (M.S.); 1614760141@qq.com (G.T.); 1752383533@qq.com (T.S.); 2360015658@qq.com (P.Y.)
*Corresponding author

***Abstract*—This study presents a three-stage optimisation framework designed for the dynamic performance enhancement of a shipboard horizontal canned-motor pump. The framework integrates high-fidelity Finite Element (FE) modelling, experimental modal validation, and topology-optimisation-based structural redesign, considering realistic installation constraints. A comprehensive whole-pump model, accounting for actual mounting conditions, is developed, and a strategy combining stiffening, lightweighting, and reinforcement is implemented to reduce structural mass while improving dynamic performance. The model's accuracy is validated through impact-hammer modal tests, with the first six natural frequencies predicted within 2% of experimental values. Modal analysis identifies a low-frequency global–high-frequency local vibration pattern, with deformation predominantly in the base transition, flange, and outlet regions. Following optimisation, the first natural frequency increases from 42.31 Hz to 76.86 Hz, and higher-order modes increase by approximately 18%, leading to more uniform mode shapes and reduced local vibration. This framework offers valuable insights for vibration mitigation and lightweight structural redesign of shipboard rotating machinery. However, internal fluid–structure interaction within the canned motor and ship-hull foundation flexibility are not incorporated in the current model, and these factors may influence low-order modal characteristics and the applicability of the results under real-world operating conditions. Future research will incorporate Fluid–Structure Interaction (FSI) modelling and shipboard experimental validation to further assess the robustness and engineering applicability of the proposed framework.**

***Keywords*—shipboard canned-motor pump, installation-constrained optimisation, modal-topology co-design, high-fidelity Finite Element (FE) modelling, frequency-separation enhancement**

## I. Introduction

Horizontal canned-motor pumps are a specialized type of pump in which the sealed motor is integrated coaxially with the hydraulic components. These pumps offer significant advantages, including "zero leakage", high reliability, and a compact structure, making them ideal for applications in nuclear power plants, petrochemical industries, high-purity fluid transportation, and liquid transfer systems on ships and offshore platforms [1]. However, under shipboard or offshore installation conditions, these pumps are subjected to complex mechanical loads, fluid disturbances, and electromagnetic excitations, which can lead to severe vibrations and local resonance. This can jeopardize the long-term operational stability and structural integrity of the equipment [2]. Therefore, dynamic characterization and vibration-control-oriented structural design for shipboard horizontal canned-motor pumps have become a key research topic for ensuring the reliability of marine platform systems.

During high-speed operation, significant structural coupling and fluid-induced pulsations can occur between the rotating and stationary components of the pump, which greatly influence its dynamic stability. Zhu *et al.* [3] observed that pressure pulsations in the rotor–stator gap induce substantial structural responses, particularly in the flange connection and casing transition regions. Hao *et al.* [4] conducted a fluid–structure coupled modal analysis of a marine centrifugal pump, demonstrating that boundary conditions and rotor mass distribution significantly impact the modal characteristics, with stress-concentrated areas often corresponding to low-order local modes. While these studies have identified key factors affecting pump vibration, including rotor–stator interaction, fluid pulsations, and varying boundary conditions, they are generally limited to the impeller or local casing, and often conducted under idealized support conditions. Consequently, they do not fully capture the coupled dynamic behavior of the entire pump–installation interface–support system, which is crucial for pumps installed on ships and offshore platforms.

Manuscript received October 13, 2025; revised November 10, 2025; accepted January 7, 2026; published March 27, 2026.

In recent years, topology optimisation techniques have become increasingly prominent in pump design, particularly in the structural optimisation of centrifugal pump rotors. Arcentales *et al.* [5] introduced a cloud-based parallel computing strategy for rotor topology optimisation, significantly improving design efficiency and enhancing the hydraulic performance of the pump. Additionally, optimisation studies on Axial Flux Motors (AFMs) and their magnetic gaps have further contributed to the theoretical understanding of pump design. Zhu *et al.* [6] demonstrated that the magnetic gap has a substantial impact on the hydraulic performance and internal flow characteristics of the pump, with an optimised gap improving both flow efficiency and overall performance. Despite significant advancements in topology optimisation and the coupling of motor design with fluid performance, most existing studies still focus on either structural or fluid-related objectives in isolation. There remains a notable gap in integrated design approaches that simultaneously combine modal characteristic identification, installation support conditions, and complete pump topology restructuring.

To accurately capture these dynamic effects and inform structural improvements, extensive modal testing techniques have been developed. Ewins [7] proposed a systematic framework for Experimental Modal Analysis (EMA), encompassing frequency response function identification, modal parameter extraction, and dynamic optimisation. He and Fu [8] further explored both time-domain and frequency-domain methods, evaluating their applicability and limitations in engineering vibration control. Maia [9] investigated coupling strategies between theoretical and measured data, providing a foundation for finite element model construction, updating, and validation. While EMA and finite element model updating techniques are now well established in structural vibration analysis, engineering studies on horizontal canned-motor pump assemblies remain scarce, particularly those that integrate installation constraints, fluid–structure interaction, and complex support conditions. There is still a lack of unified frameworks that combine high-fidelity numerical modelling, installation-interface characterisation, modal testing, and structural topology optimisation.

Finite Element Analysis (FEA) has proven to be an effective tool for identifying key modal characteristics in pump structures. Oza and Shah [10] validated their numerical results with experimental data and applied the model to optimize structural performance. Shi *et al.* [11] incorporated blade prestress effects into their analysis and examined the influence of blade thickness on modal behavior, thereby providing a theoretical foundation for designing robust impellers. While these studies have produced valuable insights at the impeller or component level, most have focused on thin-walled structures or modal analysis under idealized support conditions. There remains a significant gap in systematically extending impeller-level modal identification to whole-pump modal analysis and structural optimization.

Accurately identifying modal parameters in complex pump structures under actual operating conditions remains a challenging task. Zhang *et al.* [12] nalyzed the vibration response of a high-pressure multistage pump, emphasizing the influence of the fluid excitation spectrum on its modal behavior. Wang *et al.* [13] explored the interaction mechanisms between pressure pulsations, casing vibrations, and radiated noise, highlighting the importance of multiphysics modeling. Vinet-Huang *et al.* [14] conducted Operational Modal Analysis (OMA) under in-situ conditions, demonstrating how modal parameters evolve with the operating state and facilitating early fault detection and condition assessment. Furthermore, Jasim [15] examined impeller vibration using a combination of experimental and numerical methods, revealing a clear correlation between stiffness distribution and modal frequencies. Birajdar *et al.* [16] proposed a structural optimization approach based on hydraulic eccentricity control, which effectively reduces modal frequency drift and resonance risks caused by geometric asymmetry. Although these studies have advanced the understanding of pump dynamics in areas such as multistage pump vibration responses, pressure-pulsation–casing–noise coupling mechanisms, operational modal analysis, and local impeller vibration, most still focus on specific operating conditions or individual components, primarily emphasizing modal parameters or fault features. Integrated approaches combining operational modal analysis, high-fidelity finite element models, realistic installation constraints, and structural optimization design remain relatively scarce.

In summary, while significant progress has been made in characterizing pump vibrations using Finite Element Analysis (FEA) and Experimental Modal Analysis (EMA), most studies continue to focus on individual components or idealized support conditions. These approaches fail to adequately integrate installation constraints with the overall structural modal optimization of the pump. This issue is particularly pronounced for horizontal canned-motor pumps installed on ships, where the structure, motor, and hydraulic components are highly integrated, and the mounting interfaces are complex. To date, no systematic framework has been developed to explicitly perform modal identification and performance optimization based on the installation constraints for such shipboard pumps.

To address this gap, the present study integrates modal testing with high-fidelity numerical modeling, assuming a rigid installation foundation, to identify the global vibration characteristics of the entire pump assembly. This approach establishes an engineering basis for future research that will incorporate load-Fluid-Structure Interaction (FSI) and advanced structural optimization. Specifically, this study: (i) develops a high-fidelity whole-pump finite element model that explicitly incorporates shipboard installation constraints; (ii) validates the model through impact-hammer Experimental Modal Analysis (EMA), using identified modal strain energy to locate dynamically critical regions; and (iii) applies these results to a topology-optimization-based redesign of the base,

casing, and outlet sections, forming an installation-constrained modal-topology co-design framework for shipboard canned-motor pumps.

## II. Finite Element Theory for Structural Modal Analysis

In actual operation, a canned motor pump is not in a free state; instead, it is rigidly connected to the foundation via flanges, anchor bolts, and support brackets. Consequently, it is crucial to incorporate realistic installation boundary conditions during modal analysis to improve the alignment between simulation results and real-world operating conditions. The free vibration behavior of such linear structures can be described by the following governing equation [17]:

$$[\mathrm{M}]\{\ddot{U}(t)\} + [\mathrm{K}]\{U(t)\} = \{0\} \tag{1}$$

In Eq. (1), [M] epresents the mass matrix of the pump structure, while [K] is the stiffness matrix, which includes the additional stiffness from fixed boundary constraints. $\{\ddot{U}(t)\}$ and $\{U(t)\}$ are the nodal acceleration and displacement vectors, respectively, while {0} denotes a zero vector, indicating that the system undergoes free vibration without external excitation. It is assumed that system damping is negligible; hence, the damping matrix is excluded from the calculation of natural frequencies and mode shapes.

Assuming the structural response follows harmonic motion, the displacement can be expressed as:

$$\{U(t)\} = \{\varphi_i\} cos\omega_i t \tag{2}$$

where $\{\varphi_i\}$ represents the mode shape vector corresponding to the i-th mode, $\omega_i$ is the associated natural angular frequency (in rad/s), and $t$ is the time variable (in seconds).

By substituting Eq. (2) into the dynamic Eq. (1) eglecting the time-dependent exponential term, the standard eigenvalue problem for the modal analysis of the pump structure is derived:

$$([K] - \omega_i^2[M])\{\varphi_i\} = \{0\} \tag{3}$$

In this equation, $\omega_i^2$ represents the eigenvalue corresponding to the i-th mode, which is the square of the natural angular frequency, expressed in units of $rad^2/s^2$.

To obtain non-trivial solutions for the above linear system of equations, the determinant of the coefficient matrix must be zero:

$$det([K] - \omega_i^2[M]) = 0 \tag{4}$$

Eq. (4) guarantees the existence of non-trivial modal vectors $\{\phi\} \neq \{0\}$, which correspond to the natural frequencies $\omega$ of the structure and their associated mode shapes in physical terms.

This equation provides the standard eigenvalue formulation for the modal analysis of the pump structure. Solving it yields the complete set of natural angular frequencies $\omega_i$. The corresponding natural frequencies $f_i$ are then computed as:

$$f_i = \frac{\omega_i}{2\pi} \tag{5}$$

where $f_i$ denotes the natural frequency of the i-th mode (Hz), and $\omega_i$ is the corresponding natural angular frequency (rad/s).

To further quantify how strain, stiffness, and mass are distributed within a given mode shape, this study introduces the modal strain energy $U_r$ as a key physical indicator for structural tuning. For a linear elastic structure, the modal strain energy associated with the i-th mode can be expressed as:

$$U_i = \frac{1}{2}\int_V \varepsilon_i^T E \varepsilon_i dV \tag{6}$$

where $V$ denotes the structural volume, $\varepsilon_i$ is the strain field associated with the $i$-th mode, and $E$ is the elastic modulus tensor. Structural tuning can be viewed as redistributing the modal strain energy $U_i$ of selected modes by adjusting the stiffness and mass distribution, thereby increasing the corresponding natural frequencies and modifying the mode-shape characteristics. In this context, analysing the modal energy distribution provides a clear theoretical link to subsequent topology reconfiguration and vibration-oriented structural design.

Finite element modal analysis therefore provides a fundamental basis for evaluating structural dynamic performance. It enables the extraction of natural frequencies and mode shapes and facilitates the identification of potential modal crowding, response amplification, and resonance risk, thereby informing subsequent structural tuning and optimisation.

## III. Finite Element Modal Simulation Analysis of Canned Motor Pump

### A. Model Parameter Definition

The horizontal marine canned-motor pump considered in this study is installed on a deck foundation. Its operating parameters are as follows: a rotational speed of 3600 rpm, six impeller blades, a rotor rotational frequency of 60 Hz, and a blade-passing frequency of 360 Hz. The overall envelope dimensions are approximately 1.2 m × 0.6 m × 0.8 m, and the center of mass is located about 0.45 m above the supporting plane. The support condition is idealized as a rigid bolted connection to the foundation. A complete three-dimensional geometric model of the selected pump is constructed, as shown in Fig. 1. The mechanical properties of the materials used in the main components are summarized in Table I and are adopted as input data for the subsequent finite element modelling and modal analysis.

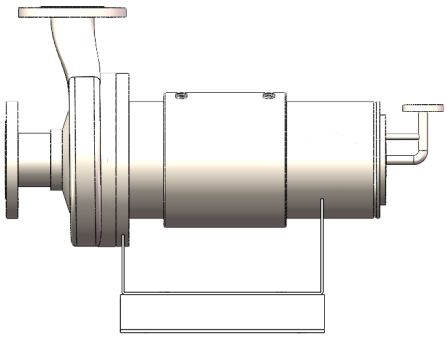

Fig. 1. Three-dimensional structural model of the canned-motor pump.

TABLE I. MATERIAL PROPERTIES OF THE CANNED-MOTOR PUMP COMPONENTS

| Parameter | Value |
|---|---|
| Elastic modulus (GPa) | 194 |
| Poisson's ratio | 0.29 |
| Density (kg/m³) | 7.93 |
| Yield strength (MPa) | 205 |

### B. Model Assumptions

In the finite element model developed in this study, the internal fluid within the canned-motor pump is not included, and the associated added-mass effect is therefore neglected. This simplification is adopted to control modelling complexity and to enable a consistent, like-for-like comparison between the baseline and optimised configurations. Prior studies have shown that accounting for fluid–structure interaction generally reduces natural frequencies relative to the corresponding dry modes owing to the added mass of the surrounding or enclosed fluid, with lower-order global modes being particularly sensitive. Meanwhile, for most operating conditions, the dominant mode-shape features and the spatial distribution of high modal strain energy remain broadly consistent between wet and dry modes [11]. Accordingly, for the present configuration and boundary conditions, incorporating the internal fluid is expected to mainly decrease the absolute values of the natural frequencies, while having a limited effect on identifying structurally weak regions—such as the base transition, flange, and outlet sections—and on the overall trend of the mode-guided optimisation strategy derived from these regions. Nevertheless, neglecting internal fluid–structure interaction constitutes an important modelling assumption and a methodological limitation of this work; its influence should be quantified in future studies using a fully coupled fluid–structure model under operating conditions representative of in-service operation.

In addition, the simplified finite element model assumes a rigid foundation for pump installation. Because the present work aims to identify the intrinsic modal characteristics of the pump structure and to perform topology-based optimisation of the pump itself, foundation compliance is not explicitly included at this stage. In shipborne and offshore applications, however, both the pump and its supporting foundation typically exhibit finite flexibility, which can have a non-negligible impact on the global low-order modes of the coupled pump–foundation system. Consequently, the rigid-foundation assumption may introduce bias in the predicted natural frequencies and mode shapes. The applicability and limitations of this assumption are discussed in the "Discussion" and "Future Work" sections, and will be further examined in subsequent studies using flexible-foundation modelling and dedicated experimental validation.

### C. Mesh Generation and Quality Control

To enhance the accuracy and robustness of the modal analysis, a high-quality finite element mesh was generated for the three-dimensional pump model in ANSYS Workbench. A mesh-independence study was then conducted to confirm that the computed results are insensitive to further mesh refinement. The resulting finite element mesh of the canned-motor pump is shown in Fig. 2, and the modelling and meshing strategy is detailed below.

#### 1) Element type selection

The higher-order tetrahedral element SOLID187 was adopted for structural discretisation. This element uses quadratic interpolation functions and provides improved surface-fitting capability, making it well suited for modal and stress analyses of geometrically complex and irregular structures. In their study of centrifugal pump impeller modal characteristics, Oza and Shah [10] reported that SOLID187 offers superior geometric adaptability and numerical robustness compared with lower-order elements, thereby improving the accuracy of natural-frequency prediction and mode-shape identification.

#### 2) Local mesh refinement strategy

Guided by the expected modal response, local mesh refinement was applied to dynamically critical regions, including the bearing seats, flange joints, and base connections, where the element size was controlled within 2.5–4 mm. In relatively less sensitive regions, such as the midsection of the pump casing, a coarser mesh (6–8 mm) was adopted to balance computational efficiency with solution accuracy.

#### 3) Mesh quality evaluation

The final finite element model comprises 332,659 nodes and 147,427 elements. The average mesh skewness is 0.21, and all Jacobian ratio values exceed 0.74, indicating high overall mesh quality. These metrics meet commonly accepted criteria for controlling element shape and distortion in high-accuracy modal simulations [18].

### D. Boundary Condition Definition

To approximate in-service boundary conditions, fully fixed constraints were applied at the bolt holes on the pump base to represent rigid anchoring to the foundation via anchor bolts. Because this stage focuses exclusively on identifying the intrinsic modal characteristics, fluid–structure interaction was not included, and a linear, undamped modal analysis was performed on the structural domain. The resulting finite element mesh of the canned-motor pump is shown in Fig. 2.

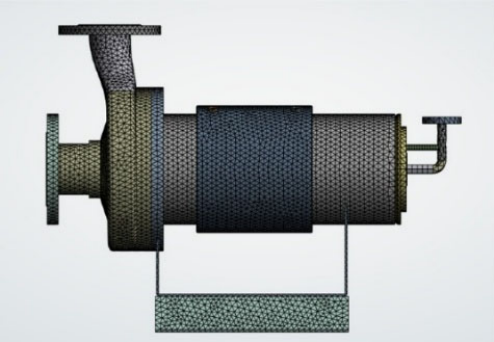

Fig. 2. Finite element mesh model of the canned-motor pump.

### E. Finite-Element Modal Simulation Results

The first six natural frequencies and the corresponding mode shapes of the pump structure were extracted using the Block Lanczos eigensolver. This algorithm offers robust convergence and numerical stability for modal analysis of large, geometrically complex structures, and has been widely adopted and validated in industrial engineering applications [19]. The simulation results, including the natural frequencies and the dominant modal characteristics, are summarised in Table II and illustrated in Fig. 3.

The simulation results indicate that the first mode is dominated by axial bending deformation localized at the bearing-support interface, implying insufficient stiffness in this region and identifying it as a primary dynamic weak point. For the second through sixth modes, pronounced local vibrations and torsional responses occur at the flange interfaces and connection regions, suggesting that limited flange stiffness and localized mass concentrations significantly influence the modal behavior. Overall, concentrated deformation is observed in the base transition zone, inlet flange, and rear pipe connection segment; these regions should therefore be prioritized in subsequent structural optimisation. These findings provide a clear physical basis for the stiffening strategy and for resonance-avoidance design measures.

TABLE II. SUMMARY OF MODAL SIMULATION RESULTS

| Mode | Natural frequency (Hz) | Modal description | Key deformation region |
|---|---|---|---|
| 1 | 42.34 | First-order axial bending mode | Bearing seat connection area |
| 2 | 110.23 | Localized torsion of the pump casing | Flange connection |
| 3 | 228.70 | Local radial vibration of the inlet flange | Inlet flange region |
| 4 | 253.00 | Coupled torsion of the inlet flange and casing | Junction of inlet and central casing |
| 5 | 306.01 | Local vibration at the outlet pipe connection | Joint between outlet pipe and end cover |
| 6 | 320.65 | Higher-order localized vibration of rear support | Rear flange and support structure |

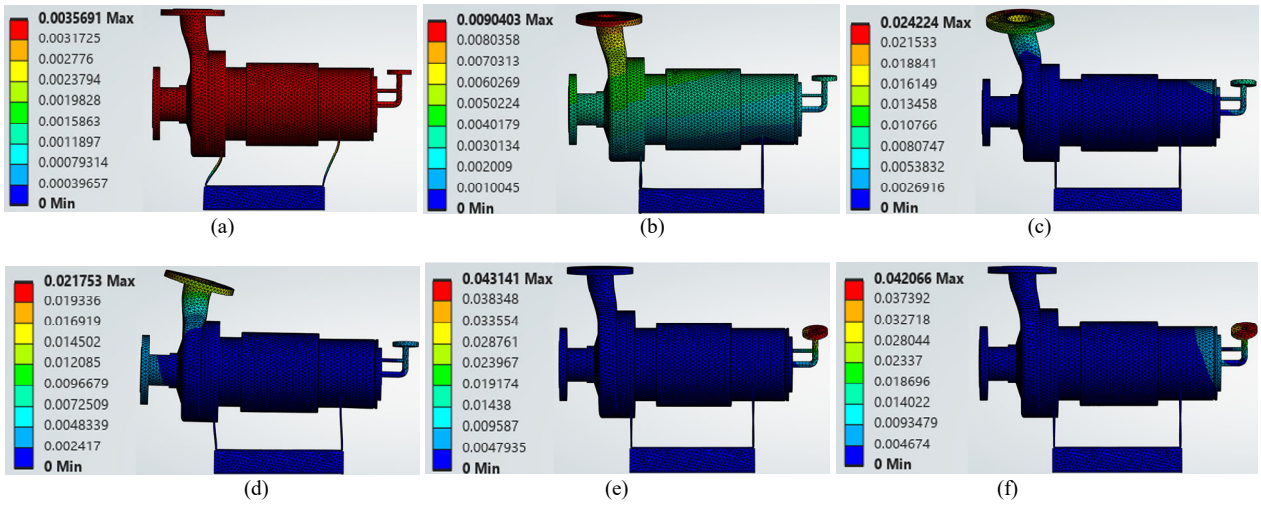


Fig. 3. Simulated mode shapes of the first six orders for the canned motor pump. (a) First-order; (b) Second-order; (c) Third-order; (d) Fourth-order (e) Fifth-order; (f) Sixth-order mode shape.

## IV. EXPERIMENTAL VALIDATION VIA IMPACT HAMMER TESTING

### A. Methodology

To validate the modal characteristics of the horizontal canned-motor pump, Experimental Modal Analysis (EMA) was performed using the impact-hammer method. This technique provides controllable excitation energy, straightforward implementation, and high accuracy for identifying low-frequency modes, and it has been widely adopted for dynamic testing of rotor–casing assemblies. Jasim *et al.* [15] successfully applied this approach to pump-impeller modal testing, further demonstrating its effectiveness and suitability for complex hydraulic structures.

A single-point excitation and multi-point response scheme was adopted to characterize the modal behavior over the pump's critical structural regions. Vibration responses were measured using PCB uniaxial accelerometers, and data acquisition and processing were conducted with a Brüel & Kjær (B&K) modal testing

system. The signals were conditioned using a preamplifier and recorded with a multichannel data acquisition unit. Frequency Response Functions (FRFs) were then computed, and modal parameters were extracted in PULSE Reflex to identify the natural frequencies and the corresponding mode shapes.

To reduce environmental disturbances and improve data reliability, each excitation point was impacted five times, and the ensemble-averaged response was used as the effective result. During testing, transient impacts were applied at key structural locations using a modal hammer, while acceleration responses were recorded simultaneously by sensors mounted at representative positions on the pump casing. The excitation and response data were subsequently imported into PULSE Reflex for frequency-domain transformation, modal identification, and multi-order curve fitting. The overall experimental procedure is illustrated in Fig. 4, which summarizes the workflow from excitation setup to modal parameter extraction.

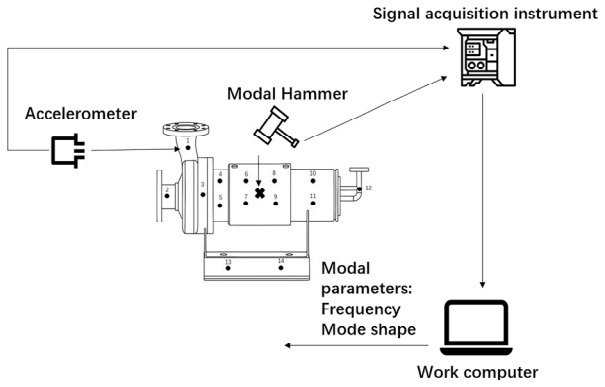


Fig. 4. Schematic diagram of the experimental modal testing procedure.

### *B. Test System Configuration and Parameter Settings*

The experimental setup comprises the excitation system, response sensors, data-acquisition modules, and a signal-analysis platform, forming a complete closed-loop testing chain. The main instruments and parameter settings are summarised in Table III, including key specifications such as excitation frequency range, sensor sensitivity, and sampling resolution, all of which satisfy the performance requirements for modal testing of the canned-motor pump.

TABLE III. EXPERIMENTAL EQUIPMENT AND CONFIGURATIONS

| No. | Equipment Name | Model /Description | Quantity |
|---|---|---|---|
| 1 | PCB uniaxial accelerometer | 353B15 | 84 |
| 2 | B&K data acquisition analyzer | 32-channel | 3 |
| 3 | B&K modal impact hammer | 8208 | 1 |
| 4 | HP mobile workstation | Data acquisition and processing | 1 |
| 5 | Signal processing software | B&K PULSE LabShop 21.0 | 1 |

A B&K Type 8208 modal hammer fitted with a rubber tip was used for excitation, with a nominal full-scale peak-force capacity of 22,240 N. Given the relatively high mass and stiffness of the shipboard horizontal canned-motor pump and the hand-held operation of the hammer, the average impact peak force was intentionally limited to approximately 300 N (±30 N). This level was selected to ensure controllable and repeatable impacts while providing sufficient low-frequency excitation for reliable identification of the low-order modes.

Vibration responses were measured using a PCB 353B15 uniaxial accelerometer with a sensitivity of 1 mV/(m·s$^2$). Owing to its wide frequency bandwidth and excellent linearity, this sensor is suitable for dynamic measurements on medium- and large-scale structures.

Data acquisition and analysis were conducted using a B&K Type 3560C multichannel dynamic signal analyzer integrated with the PULSE LabShop 21.0 platform for real-time signal conditioning and frequency-domain analysis. The test frequency range was set to 0–400 Hz with a resolution of 625 mHz, which meets the accuracy requirements for identifying the first six natural mode.

To enable synchronized multi-axis response measurements, tri-axial sensor groups (three uniaxial accelerometers) were mounted along the X, Y, and Z directions on common mounting blocks. The sensors were bonded to the pump surface using adhesive to ensure stable signal transmission (Fig. 5). Measurement points were laid out based on structural symmetry and modal-sensitivity considerations, covering critical regions including the pump mid-section, inlet flange, and outlet flange. In total, 28 measurement points were deployed, as shown in Fig. 6.

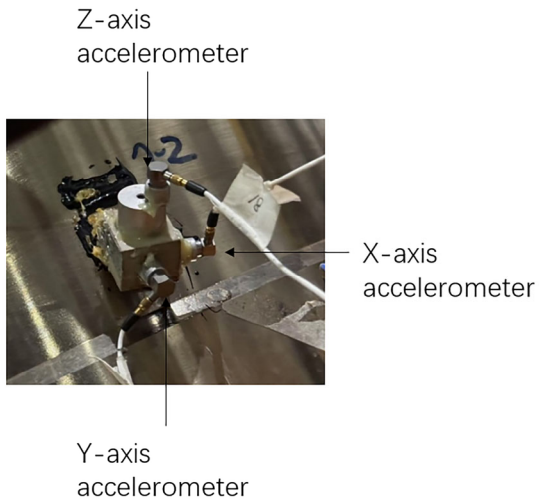


Fig. 5. Schematic diagram of sensor installation for measurement points.

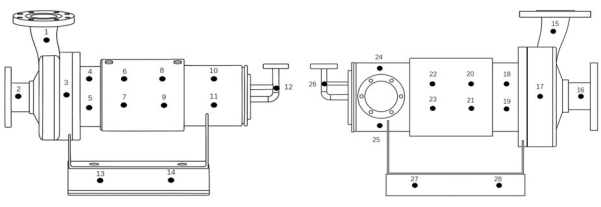

(a) (b)

Fig. 6. Schematic diagram of measurement point layout. (a) Front, (b) Rear view.

### C. Comparison between Experimental and Simulation Results

A comparative analysis was performed between the impact-test measurements and the finite element predictions for the first six modal frequencies of the canned-motor pump. The Modal Power Indication Function (MPIF) curves are shown in Fig. 7, and the corresponding frequency comparison is summarized in Fig. 8.

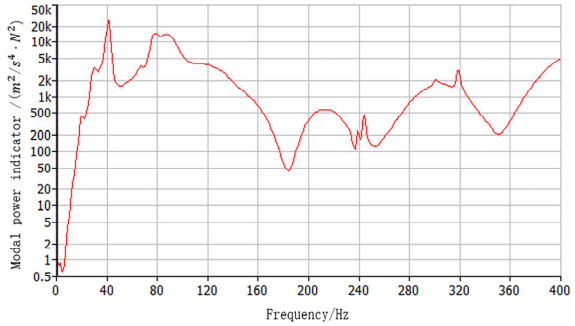


Fig. 7. Modal Power Indicator Function (MPIF) curves for the first six modes.

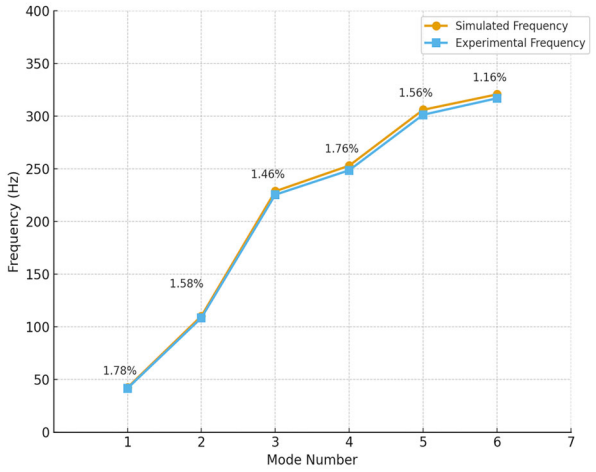


Fig. 8. Comparison chart of test and simulation errors.

As shown in Fig. 7, the measured Modal Power Indicator Function (MPIF) curves exhibit distinct response peaks at approximately 42, 110, 228, 253, 306, and 320 Hz, which are consistent with the FE results. The peaks are clearly separated in the frequency domain, with no evident overlap or aliasing, confirming reliable experimental identification of the corresponding modes. Collectively, these results support the reliability of the FE-extracted modal parameters and their applicability for subsequent engineering analysis and optimisation.

As shown in Fig. 8, the experimentally identified natural frequencies agree closely with the Finite Element (FE) predictions, with relative errors below 2% for all six modes. This level of agreement indicates that the FE model—including the assigned material properties, boundary conditions, and mesh discretisation—is both accurate and representative.

Overall, the numerical and experimental modal results are highly consistent, validating the finite element modelling approach and the experimental procedure adopted in this study, and providing a robust basis for subsequent structural dynamic optimisation and vibration-mitigation design.

## V. Structural Optimisation

### A. Optimization Objectives and Strategy

Horizontal canned-motor pumps operating at high rotational speeds are subjected to periodic excitations arising from electromagnetic forces and fluid pulsations. If the structural natural frequencies coincide with these excitation frequencies, resonance may occur, leading to excessive vibration, fatigue damage, and potentially premature failure. Accordingly, increasing the lower-order natural frequencies and improving the mode-shape distributions are critical for ensuring dynamic stability and operational reliability.

According to structural dynamics theory, the natural frequencies of a system are governed by its stiffness matrix $K$ and mass matrix $M$, which together define the generalized eigenvalue problem expressed as:

$$\omega_i = \sqrt{\frac{\Phi_i^T K \Phi_i}{\Phi_i^T M \Phi_i}} \tag{7}$$

In Eq. (7), $\omega_i$ denotes the $i$ th natural angular frequency, $\Phi_i$ is the corresponding mode-shape vector, and $\Phi_i^T$ is its transpose. This eigenvalue relationship indicates that increasing a structure's natural frequency can be achieved by increasing its effective stiffness or reducing its effective mass, with the greatest impact typically occurring in regions of concentrated modal strain energy [7, 17].

To increase the low-order natural frequencies while meeting lightweight design requirements, this study adopts a stiffening–lightweighting–reinforcing strategy. The approach targets modal-sensitive regions—such as the base transition zone, flange connections, and the rear small-pipe section—where local stiffening is combined with selective mass reduction in non-load-bearing areas to improve overall modal performance.

Building on the above analysis, a topology-optimisation model was formulated in ANSYS Workbench with the first natural frequency as the objective. The design domain was discretised into finite elements, and the relative density of each element was defined as $\rho_e \in [\rho_{\min}, 1]$. The design variables are the element densities $\rho_e$ within the design domain. The objective is to maximise the first natural frequency $\omega_1(\rho)$, subject to the constraint that the total structural mass does not exceed 95% of the original mass. The resulting optimisation problem can be written as:

$$max_{\{pe\}} f(\rho) = \omega_1(\rho) \tag{8}$$

$$s.t. \sum_{e=1}^{N} \rho_e V_e \tau \leq 0.95 \sum_{e=1}^{N} V_e \tag{9}$$

$$\rho_{min} \leq \rho_e \leq 1 \tag{10}$$

where $N$ is the total number of elements in the design domain, and $\rho_{\min}$ is the minimum normalised density, introduced to avoid singularity of the stiffness matrix and to retain the stiffness contribution of "very weak material".

To drive the density field towards a 0/1 distribution and suppress intermediate densities, the elastic modulus of the material is interpolated using the standard SIMP scheme:

$$E(\rho_e) = E_{min} + \rho_e^p (E_0 - E_{min}) \tag{11}$$

where $E_0$ is the Young's modulus of the solid base material, and $E_{\min}$ is the equivalent elastic modulus assigned to the "very weak" material, which is usually taken as

$$E_{min} = \rho_{min} E_0 \tag{12}$$

In this study, the minimum normalised density is set to $\rho_{\min} = 1.0 \times 10^{-3}$, and the penalisation factor is chosen as $p = 3$. Under this interpolation scheme, high-density elements contribute significantly to the overall stiffness, while intermediate-density elements are penalised, thereby promoting a clear 0–1 topology layout under the combined constraints of frequency and mass.

To suppress checkerboard patterns and other numerical artefacts, and to control the minimum feature size, an automatically controlled density-filtering scheme was applied during the topology optimisation. The design variables were weighted and averaged within a prescribed spatial neighbourhood to smooth the density field, ensuring that the resulting topology exhibits reasonable geometric length scales and improved manufacturability.

The maximum number of optimisation iterations was set to 500, and convergence was defined as a relative change of less than 0.1% in the objective value between two successive iterations. The iteration history indicates that this criterion was essentially satisfied after approximately 13–14 iterations, with only negligible variations thereafter. The optimisation was therefore terminated at the 16th iteration, at which point the target frequency had stabilised and the topology optimisation was considered converged.

To verify the stability of the topology-optimisation process and compliance with the imposed constraints, the convergence histories of the objective function and the mass-constraint response are presented in Figs. 9 and 10, respectively. As shown in Fig. 9, the objective decreases rapidly during the initial iterations and, after approximately the 13th–14th iterations, its variation becomes small and remains below the convergence-threshold line, indicating that the optimisation has effectively converged by the 16th iteration. Fig. 10 indicates a brief overshoot of the mass constraint in the early iterations; however, from the 3rd iteration onward it decreases and stabilises at approximately 94.2%, which is essentially consistent with the prescribed upper bound of 94.159%. Collectively, these results demonstrate that the proposed topology-optimisation model converges under the specified mass constraint and yields a reliable structural configuration for subsequent modal-performance assessment.

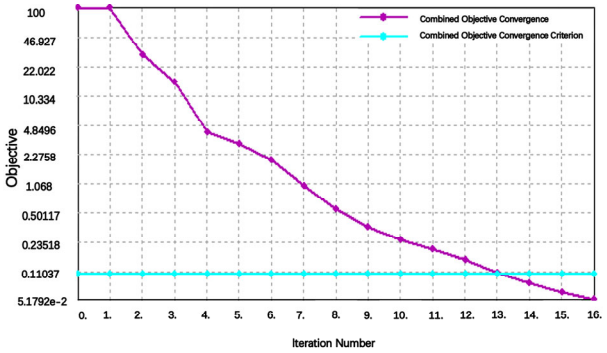


Fig. 9. Convergence curve of combined objective.

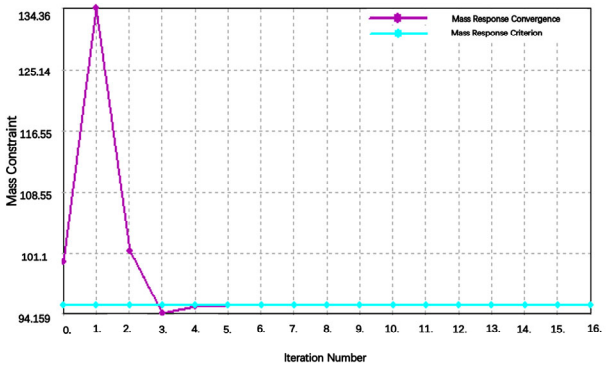


Fig. 10. Convergence curve of mass response.

As illustrated in Fig. 11, the optimised density field highlights high-density regions as primary load-bearing paths, whereas low-density regions represent candidates for material removal. The strain-energy density distribution further identifies the base transition region, central shell, and tail-end connection as the dominant modal-control zones. The resulting material layout is consistent with the prior modal-sensitivity analysis, supporting the effectiveness of the proposed topology-optimisation approach through the mechanism of stiffness reconfiguration and mass redistribution. These findings provide direct guidance for subsequent local stiffening and weight-reduction design.

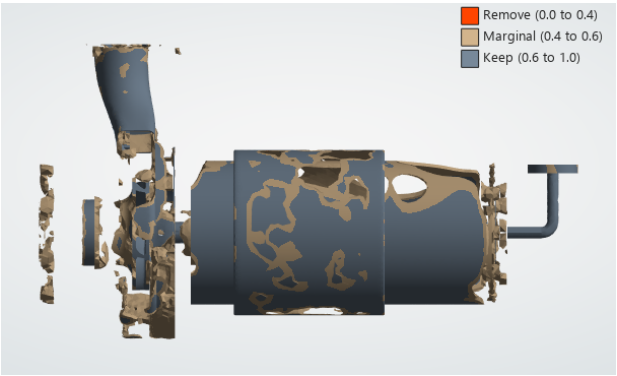


Fig. 11. Topology-optimised element density distribution.

Based on the topology-derived density distribution and the identified modal strain-energy concentration zones, three targeted optimisation measures were implemented.

*1) Base-support stiffening*

Modal analysis indicates that the peak displacement of the first mode is concentrated in the transition region between the base and the pump body, suggesting high sensitivity to dynamic excitation. To address this weak region, triangular stiffening ribs were introduced to enhance local bending stiffness. This modification increases the effective stiffness and thereby elevates the first natural frequency [7, 17]. After optimisation, the first natural frequency increased by 81.7% relative to the original design, confirming that local stiffening can effectively reduce resonance susceptibility.

*2) Mass reduction in non-load-bearing zones*

The topology-derived density field indicates that the mid-section and tail region of the pump casing correspond to low-density areas. When interpreted together with the modal strain-energy distribution, these regions can be classified as "low-energy–high-mass" zones. According to topology-optimisation principles, reducing wall thickness in such zones can lower the effective mass while leaving the global stiffness largely unchanged, thereby shifting the natural frequencies upward [5]. In this study, the casing wall thickness in these regions was reduced from 10 mm to 6 mm. Relative to the original structure, the second to fourth natural frequencies increased by 10%–25%. Although this represents a 40% thickness reduction, the modification was intentionally confined to the identified low-energy, high-mass zones to improve dynamic performance while maintaining structural functionality. Nevertheless, wall-thickness reduction may introduce risks related to load-carrying capacity, buckling resistance, and fatigue life. Accordingly, future work will include dedicated assessments of strength, stability, and fatigue to ensure an appropriate balance between vibration performance and structural safety.

*3) Outlet-section reinforcement for vibration suppression*

Higher-order modes exhibit pronounced local bending in the rear outlet pipe, indicating insufficient stiffness in this region. To enhance bending resistance, the pipe outer diameter was increased from 80 mm to 110 mm, accompanied by an increase in wall thickness. According to Timoshenko beam theory, the bending natural frequency scales with the square root of the area moment of inertia, suggesting a theoretical upper bound of approximately a 1.55-fold increase [20]. After optimisation, the modal frequencies associated with this region increased by 9.7% and 21.5%, respectively. Although these gains remain below the theoretical upper bound, the high-frequency local vibrations were substantially suppressed, demonstrating the effectiveness and practical feasibility of the proposed reinforcement.

It should be noted that the topology-optimisation model employed in this study targets the relationship between natural frequency and mass, and does not explicitly impose stress- or strength-related constraints. This simplification reflects the present focus on improving modal performance and increasing resonance margins through moderate shell thinning and local stiffening. In addition, the prototype canned-motor pump has already undergone conventional strength design and verification. Nevertheless, the optimised configuration will require further verification, including checks for static strength, buckling, and fatigue, in future work. Accordingly, the results reported herein primarily demonstrate trends in frequency enhancement and mass redistribution, whereas strength and durability under high-load operating conditions will be addressed in subsequent studies.

Overall, the combined measures—base stiffening, selective mass reduction, and outlet-section reinforcement—produce a systematic improvement in modal characteristics: natural frequencies increase across all modes, critical deformation becomes more localized and better controlled, and the global dynamic behavior of the system is enhanced. A structural comparison of the configurations before and after optimisation is shown in Fig. 12.

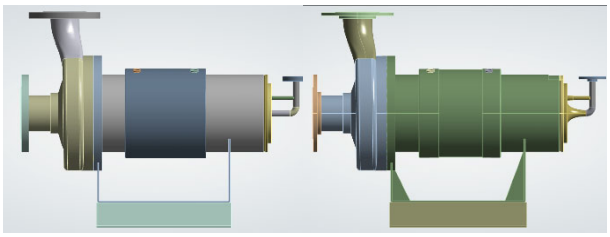

(a) (b)

Fig.12 Structural comparison before and after optimization. (a) Original (b) Optimised model.

## *B. Modal Analysis Validation of the Optimized Structure*

Modal analysis of the optimised structure was performed in ANSYS to extract the first six natural frequencies and their corresponding mode shapes. The mode shapes are presented in Fig. 13, and the relative increases in natural frequency are summarised in Fig. 14.

After optimisation, the first and second natural frequencies increase to 76.86 Hz and 127.57 Hz, respectively. This increase enlarges the separation from the dominant excitation components (rotor frequency of 60 Hz and blade-passing frequency of 360 Hz) and reduces the likelihood of resonance in the frequency domain.

All extracted natural frequencies are higher than those of the baseline configuration. In the low-order modes, global deformation in the base region is substantially reduced, indicating an enhanced stiffness response. In the higher-order modes, pronounced local vibrations are effectively suppressed and the mode shapes become more uniformly distributed, resulting in increased modal margins and improved resistance to resonance under typical operating conditions.

Overall, the proposed optimisation scheme achieves coordinated improvements in modal performance and mass distribution while preserving global structural integrity, providing a more robust structural basis for the long-term stable operation of the canned-motor pump under high-speed, high-excitation conditions.

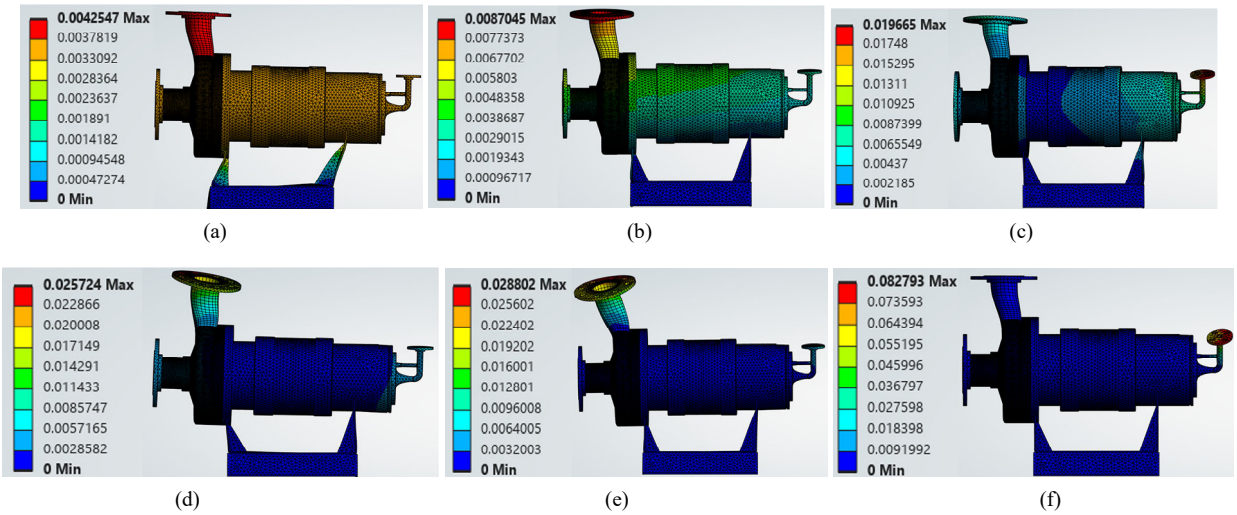


Fig. 13 First six mode shapes (a) First mode; (b) Second mode; (c) Third mode; (d) Fourth mode; (e) Fifth mode; (f) Sixth mode of the pump after optimization.

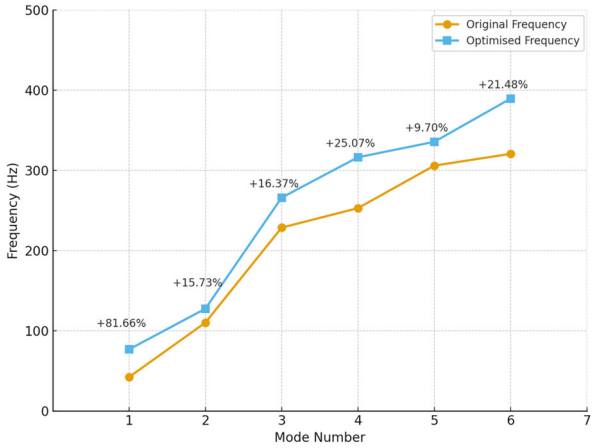


Fig. 14 Comparison chart of natural frequency improvement after optimization.

## VI. Conclusion

To improve the dynamic robustness of a shipboard horizontal canned-motor pump under realistic installation constraints, this study proposes and validates a modal-guided optimisation framework integrating installation-representative whole-pump Finite Element (FE) modelling, impact-hammer experimental modal analysis, and topology-optimisation-based structural redesign. The main conclusions are as follows.

(1) A whole-pump FE model consistent with the adopted mounting configuration was established and validated via impact-hammer modal testing. The first six natural frequencies were predicted within 2% of the measurements, indicating that the model is sufficiently accurate for modal interpretation and design iteration.

(2) Modal diagnosis of the baseline design reveals a transition from low-frequency global deformation to high-frequency local vibration. Deformation concentrates mainly in the base transition, flange, and outlet regions, indicating that these features govern local compliance and dominate resonance susceptibility.

(3) Based on the identified modal weaknesses, a stiffening–lightweighting–reinforcing redesign strategy was implemented in conjunction with topology optimisation to enable efficient material redistribution. The first natural frequency increased from 42.31 Hz to 76.86 Hz, and higher-order natural frequencies improved by approximately 18% on average.

(4) Beyond frequency elevation, the redesign improves modal quality by reducing local deformation concentration and producing more uniformly distributed mode shapes in the critical regions. From a practical perspective, the results support a vibration-oriented guideline: prioritise stiffness tailoring along principal load-transfer paths at installation interfaces while removing low-contribution material elsewhere to increase low-order frequency margins under constrained shipboard layouts.

(5) Overall, the proposed workflow provides a transferable reference for vibration mitigation and lightweight structural redesign of shipboard rotating machinery where realistic installation constraints must be explicitly represented during optimisation.

These conclusions are drawn from structural modal characteristics under the current modelling assumptions. Internal fluid–structure interaction within the canned cavity and ship-hull foundation flexibility were not included and may influence low-order modal characteristics in service. Future work will incorporate coupled multiphysics modelling and shipboard validation to quantify robustness and further substantiate engineering applicability.

## Conflict of Interest

The authors declare that no financial or non-financial conflicts of interest exist during the research process that could affect the integrity of the research findings. None of the authors have received financial support, royalties, or other benefits from any company, institution, or individual

directly related to the content of this article. The experiments, analyses, and conclusions of this study were based on independent and objective scientific judgment to ensure academic integrity and research fairness.

## AUTHOR CONTRIBUTIONS

X.S. conducted the research, performed the experiments, and wrote the initial draft of the paper. D.Y. provided guidance and supervision throughout the project M.Y.S, G.C.T, T.M.S, and P.H.Y assisted in data collection and resources. All authors reviewed and approved the final manuscript.

## FUNDING

This work was supported by the Fundamental Research Project of the Education Department of Liaoning Province (Open Bidding and Task-Based Program) under Grant No. LJKFZ20220289; and by the Liaoning Provincial Science and Technology Program Joint Plan (Natural Science Foundation—General Program) under Grant No. 2025-MSLH-030, "Key Technologies for Vibration Suppression of High-Precision Operation Robots".

## REFERENCES

[1] Z. Chen, Y. Gu, W. Lu, L. Zhang, D. Zhu, and Z. Zhou, "Characterization of solid-liquid two-phase flow in a canned-motor pump for marine vehicles based on the Euler-Lagrange method," *Ocean Eng.*, vol. 335, 121726, 2025. doi: 10.1016/j.oceaneng.2025.121726

[2] C. Dai, Y. Zhang, Q. Pan, L. Dong, and H. Liu, "Study on vibration characteristics of marine centrifugal pump unit excited by different excitation sources," *J. Mar. Sci. Eng.*, vol. 9, no. 3, 274, 2021. doi: 10.3390/jmse9030274

[3] Z. Yue, Z. Jige, Y. Junlian, C. Hui *et al.*, "Pressure pulsation characteristics between the rotating and stationary parts of a shielded nuclear main pump," *At. Energy Sci. Technol.*, vol. 48, no. 9, pp. 1576–1582, 2014. doi: 10.7538/yzk.2014.48.09.1576

[4] H. Haoqin, L. Houlin, W. Yong, D. Hanwei, and J. Linling, "Stress-strain and modal analysis on rotor of marine centrifugal pump based on fluid-structure interaction," *Trans. Chin. Soc. Agric. Eng.*, vol. 30, no. 15, pp. 98–105, Aug. 2014. doi: 10.3969/j.issn.1002-6819.2014.15.014

[5] X. A. Arcentales, D. A. Arcentales, and W. Montealegre, "Design of rotors in centrifugal pumps using the topology optimization method and parallel computing in the cloud," *Machines*, vol. 13, no. 4, 307, 2025. doi: 10.3390/machines13040307

[6] Q. Zhu, Y. Gu, and J. Bian, "Impact of the magnetic gap in submerged axial flux motors on centrifugal pump hydraulic performance and internal flow," *Machines*, vol. 13, no. 8, 721, 2025. doi: 10.3390/machines13080721

[7] D. J. Ewins, *Modal Testing: Theory, Practice and Application*, Hoboken, NJ, USA: John Wiley & Sons, 2009.

[8] Z.-F. Fu and J. He, *Modal Analysis*, Oxford, U.K.: Elsevier, 2001.

[9] M. N. M. Maia, *Theoretical and Experimental Modal Analysis*, Taunton, Somerset, England: Research Studies Press, 1997.

[10] M. N. Oza and D. S. Shah, "Theoretical and experimental modal analysis of centrifugal pump radial flow impeller," *IOP Conf. Ser., Mater. Sci. Eng.*, vol. 992, no. 1, 012003, 2020. doi: 10.1088/1757-899X/992/1/012003

[11] L. Shi, J. Zhu, L. Wang, S. Chu, F. Tang, and Y. Jin, "Comparative analysis of strength and modal characteristics of a full tubular pump and an axial flow pump impellers based on fluid-structure interaction," *Energies*, vol. 14, no. 19, 6395, 2021. doi: 10.3390/en14196395

[12] Y. Zhang *et al.*, "Vibration analysis of a high-pressure multistage centrifugal pump," *Sci. Rep.*, vol. 12, no. 1, 20293, 2022. doi: 10.1038/s41598-022-22605-2

[13] C. Wang, X. Chen, N. Qiu, Y. Zhu, and W. Shi, "Numerical and experimental study on the pressure fluctuation, vibration, and noise of multistage pump with radial diffuser," *J. Braz. Soc. Mech. Sci. Eng.*, vol. 40, no. 10, 481, 2018. doi: 10.1007/s40430-018-1355-6

[14] V. Viet-Hung, B. Bechir, T. Marc, and J. Pierre, "Operational modal analysis on a pump operating at varying speeds: an industrial history case," *Mech. Ind.*, vol. 17, no. 1, 105, 2016. doi: 10.1051/meca/2015043

[15] H. Jasim, "Experimental and FEM vibration analysis of impellers used for water pump," *Int. J. Eng. Appl. Phys.*, vol. 3, no. 2, pp. 689–699, 2023.

[16] R. S. Birajdar, A. A. Keste, and S. H. Gawande, "Critical hydraulic eccentricity estimation in vertical turbine pump impeller to control vibration," *Shock Vib.*, vol. 2021, 6643282, 2021. doi: 10.1155/2021/6643282

[17] J. Humar, *Dynamics of Structures*, 3rd ed. Boca Raton, FL, USA: CRC Press, 2012.

[18] C. Pisarciuc, I. Dan, and R. Cioară, "The influence of mesh density on the results obtained by finite element analysis of complex bodies," *Materials*, vol. 16, no. 7, 2555, Jan. 2023. doi: 10.3390/ma16072555

[19] D. M. El-Gazzar, "An integrated study for solving high vibration problem of a deep well turbine pump," *Diagnostyka*, vol. 24, no. 2, pp. 1–9, 2023.

[20] S. P. Timoshenko and J. M. Gere, *Theory of Elastic Stability*, 2nd ed. Mineola, NY, USA: Dover Publications, 2012.